# Dynamic model of a vortex-induced energy converter

***G. Manfrida[a], M. Rinchi[b], G. Soldi [c]***

*[a] Dipartimento di Ingegneria Industriale, Università di Firenze, Firenze, Italy, giampaolo.manfrida@unifi.it*
*[b] Dipartimento di Ingegneria Industriale, Università di Firenze, Firenze, Italy, mirko.rinchi@unifi.it*
*[c]Dipartimento di Ingegneria Industriale, Università di Firenze, Firenze, Italy, guido.soldi@stud.unifi.it*

**Abstract:**
Vortex-Induced Energy Converters (VIECs) are attracting the attention of researchers looking for Energy-Harvesting systems in the marine environment. These energy converters, while probably less efficient than many other specialized devices, have very few moving parts and are particularly suitable for operation in harsh environments, such as those encountered in the ocean and in offshore platforms. The principle of operation of VIECs is tapping the transverse vibration of a blunt slender body immersed in a stream, induced by unsteady flow separation (Von Karman vortex street). The simplest device is an array of cylinders: under specific conditions and with careful design, it is possible to work close to resonance and thereby to obtain large amplitudes of oscillation, which are converted into electricity by suitable devices (linear electrical generators or piezoelectric cells). The system has been developed experimentally at University of Michigan, with several patents pending and scientific material published on preliminary tests: it appears that a fundamental comprehensive model is missing from the technical literature. A model of the system was thus developed, resulting in a nonlinear dynamic mathematical formulation; this last is solved in the time domain using Matlab/Simulink programming. The sensitivity of the efficiency to the main design variables is investigated. The results demonstrate that the efficiency and power density are not attractive for the typical Mediterranean sea conditions: however, as energy can be harvested over large surfaces, the system appears to deserve attention.

**Keywords:**
Energy Harvesting, Tides, Streams, Vortex-Induced Energy Converters.

## 1. Sea Energy Harvesting and Vortex Induced Vibration Converters

Most of the devices that extract kinetic energy from the sea/rivers are water mills, water turbines or moving structures that use buoys oscillation or other mechanical principles. The Vortex-Induced Energy Converters seem to be unique in their fundamental working principle, that is to enhance, rather than to suppress, the effect of vortex-induced vibration (which is frequently cause of high damage to aero, civil, mechanical, marine, offshore and nuclear engineering structures) in order to convert the energy of a fluid stream in electricity [1-3]. The VIVACE (Vortex Induced Vibration Aquatic Clean Energy) device was invented in 2008 by Bernitsas and Raghavan and patented through the University of Michigan in 2009 [2]. It converts the energy of ocean/river streams into electricity. In its simplest structure, a module of the VIVACE Converter presents a rigid cylinder of circular section mounted on springs and connected to a Power Take-Off (PTO) system through a transmission mechanism [4]. The presently applied PTO system consists of a gear-belt transmission system and an off-the-shelf rotary generator; alternatives such as an hydraulic system, a linear generator [4] or a piezoelectric converter are possible.
Vortex-Induced Converters use Vortex Induced Vibrations (VIV) from fluid flow to produce energy successfully with a high power conversion ratio. VIV involves the synchronization between vortex shedding and body (i.e. cylinders or spheres) oscillations. This interaction between the fluid and the structure occurs due to non-linear resonance of bodies (cylinders or spheres) through vortex shedding synchronization, which is also called lock-in.
A typical VIV converter has a scalable geometry and can extract energy from currents with velocities from 0.3 to 9 km/h and above (0.5-5 knots) [2]. It is a robust system, because it presents

low sensitivity to environmental conditions, since the vortex synchronization occurs over a relatively wide range of frequencies and not just at natural frequencies as in linear resonance [4].

## 2. Vortex Shedding Background

In the case of a stationary cylinder, the unsteady forces due to flow separation in turbulent flow show a typical power spectrum with a peak at a frequency $f_{St}$, called Strouhal frequency:

$$f_{St} = \frac{U\,St}{D}\,, \tag{1}$$

where *St* is the Strouhal number. The Vortex Shedding occurs up to very high values of *Re* (*Re* = $10^4$-$10^5$). In this range, in the general case of bluff bodies, the value of St goes from 0.2 to 0.3. From (1) it is thus possible to determine the frequency of vortex shedding, when the flow velocity *U* and the reference dimension *D* of the body (the diameter for a circular shape) are known. Supposing that the body has a mass *m*, and is undamped and elastically supported by a spring of stiffness *k*, the natural/resonance vibration frequency is defined as:

$$f_0 = \frac{\omega_0}{2\pi} = \frac{1}{2\pi}\sqrt{\frac{k}{m}} \tag{2}$$

When the body is free to vibrate perpendicularly to the vein and $f_0$ coincides with the frequency $f_{St}$, it begins to fluctuate significantly, excited in resonance.

In the case of a fixed cylinder, the vortex shedding occurs disorderly in various sections along the profile of the cylinder creating random forces; when the body is allowed the transverse degree of freedom and the frequency of vibration of the body coincides with $f_{St}$, the vortex detachment starts its synchronization with the vibration of the body. The synchronism between the vortex shedding and the oscillation results in the increase of the intensity of the alternating lift force. This synchronism is maintained when the vein velocity, *U*, increases within a certain interval, the so-called synchronization field.

The Strouhal relationship (1) shows that the vortex shedding frequency $f_V$ varies linearly with the incident flow velocity *U*. In condition of resonance, there is a synchronism between the vortex shedding and the vibration of the structure ($f_{cyl} = f_V$). This synchronism is maintained even if the stream velocity varies within a synchronization range. This phenomenon is called lock-in.

Fig. 1 shows the fundamental issue of Vortex-Induced Vibration Synchronization in terms of a reduced frequency/reduced velocity graph. The reduced velocity is defined as:

$$U^* = \frac{U}{f_0 D} \tag{3}$$

The non-dimensional mass *m** can be defined as the ratio between the total mass of the oscillating structure *m*, and the mass $m_d$ of the fluid displaced:

$$m^* = \frac{m}{m_d} \tag{4}$$

where the total mass of the oscillating structure *m* includes the mass of the cylinder and a certain fraction of other oscillating components (e.g. 1/3 of the mass of the spring) [3].

As it can be seen from Fig. 1, the Strouhal relationship is violated within the synchronization range, since the frequency of vortex detachment $f_V$ remains constant as the flow velocity increases. Accordingly, Khalak and Williamson [5] define synchronization as the "matching of the frequency of the periodic wake vortex mode with the body oscillation" or $f_V$=$f_{cyl}$.

Fig. 1 also shows that the phenomenon of lock-in varies depending on *m**. Actually, when *m** presents high values, $f_{cyl}$ returns a value close to the natural vibration frequency of the body $f_0$, and the lock-in range is developed around $f^* = f_{cyl}/f_0$ approximately equal to unity [6-7]. For low values of non-dimensional mass, instead, the body oscillates with $f^*>1$, and the synchronization range extends over a wider range of *U** [4, 7-8].

Moreover, $f^*$ may differ significantly from the theoretical unit value also because, as demonstrated in number of recent experimental reports, synchronization is the "matching of the frequency of the periodic wake vortex mode with the body oscillation frequency" [5] and at least four wake patterns that are different from the classical Karman vortex street have been experimentally observed.
Typically, an oscillation amplitude equal to a fraction of the diameter $D$ is observed, and a maximum takes place for certain values of the parameter $U^*$ within the synchronization range.
At the end of the synchronization interval, the frequency of detachment returns abruptly to the value expected from the Strouhal relationship (Fig. 1).

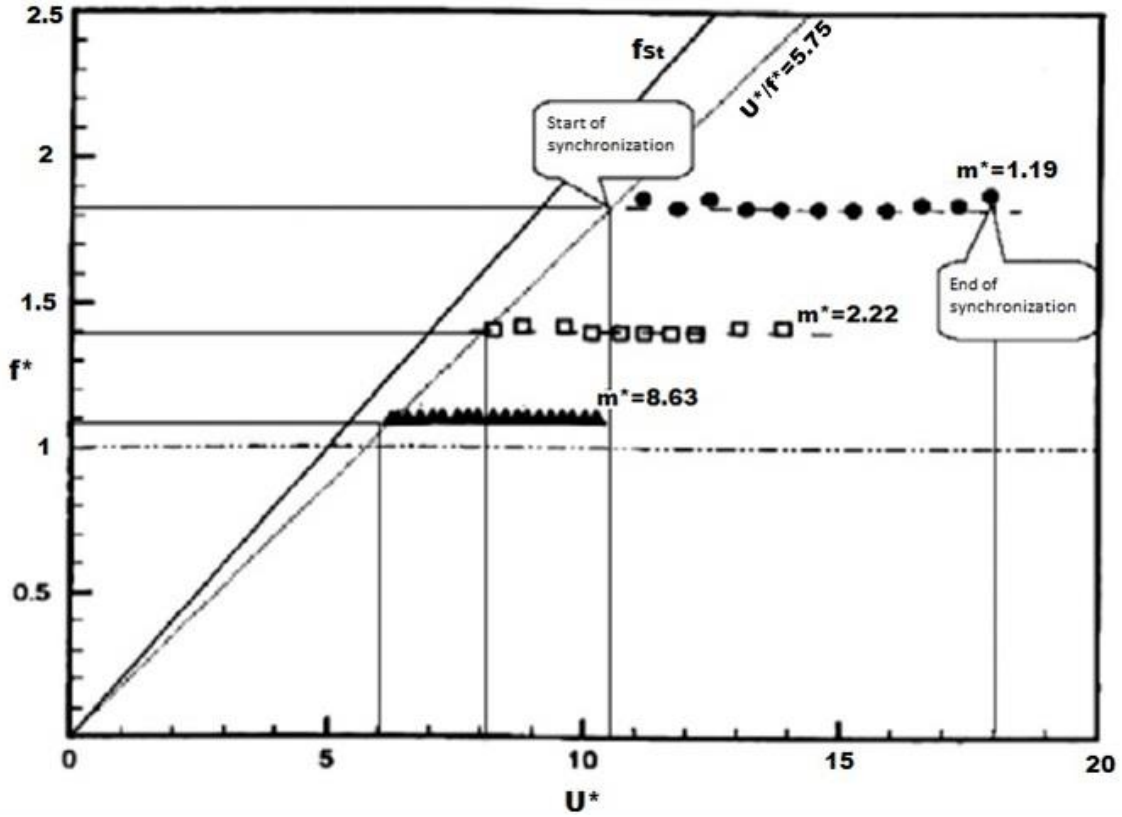


*Fig. 1. Dimensionless cylinder oscillation frequency for different values of non-dimensional mass coefficient as a function of flow non-dimensional velocity U*; reproduced from [4].*

Another relevant issue is to identify the Reynolds regime that is more advantageous for system operation. Following the classification in [9], confirmed by experiments, it is convenient to operate the system in the region of maximum lift coefficient $C_L$, which is typically delimited in the range $2x10^4<Re<3.5x10^5$. This determines in practice the diameter $D$ once the stream velocity is specified.

# 3. Mathematical Model

A simple scheme of a single module is represented in Fig. 2. The cylinder is placed with its axis in the $z$ direction (perpendicular to the flow velocity $U$, with direction $x$). It is free to oscillate in the $y$ transverse direction. From the mathematical point of view, the structure can be analyzed as a simple mass-spring-damper model.

As described in [4], the total damping parameter $c_{tot}$ can be subdivided in four main components:

$$c_{tot} = c_{sys} + c_{tra} + c_{gen} + c_{harn} \quad (5)$$

For the purpose of the present simulation, the knowledge of $c_{tot}$ is sufficient; however, it is important to underline that the system should be designed so that the real assembly, including the four contributions, realizes the correct value of $c_{tot}$.

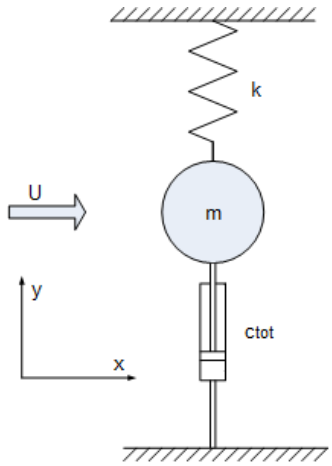


*Fig.2. Simple Schematic for Vortex-Induced Converter Dynamics.*

## 3.1. Dynamic Equation

In the present forced vibrations context, the system is excited by an external force and vibrates due to its persistent action. The motion of the cylinder in the *y*-direction (Fig.2) may be described by the simple second order equation:

$$m\ddot{y} + c_{tot}\dot{y} + ky = F_{fluid} \quad (6)$$

where *y* is the vibration amplitude in the direction perpendicular to the flow and to the cylinder axis; *m* is the equivalent mass of the oscillating system, *k* is the spring stiffness, $c_{tot}$ is the total damping coefficient and $F_{fluid}$ is the force exerted by the fluid on the body, in the *y*-direction.

The fluid/cylinder interaction force may be subdivided in an aerodynamic component (depending on velocity squared) $F_{aer}$, and in an added inertia one $F_{addin}$, originating by the inertial force of the fluid displaced by cylinder oscillations, as analyzed by [7-8]. Therefore equation (6) can be re-written as:

$$m\ddot{y} + c_{tot}\dot{y} + ky = F_{aer} + F_{addin} \quad (7)$$

The aerodynamic force may be defined as:

$$F_{aer} = \frac{1}{2} C_L \sin(2\pi f_V t + \varphi)\rho U^2 DL \quad (8)$$

where $C_L$ is the lift coefficient and $\varphi$ the phase shift between the fluid forcing and cylinder displacement. In particular, for the Reynolds range between $5.4\text{x}10^3$ and $2.2\text{x}10^5$, the lift coefficient [10] is approximately equal to:

$$C_L \cong 0.52\text{-}0.06 * \left(\log\left(\frac{\mathrm{Re}}{1{,}6\times 10^3}\right)\right)^{-2.6} \quad (9)$$

The added inertia force may be defined in terms of the added mass, $m_a$:

$$F_{addin} = -m_a\ddot{y} \quad (10)$$

The added mass is defined in [4] as "the impulse given to the fluid during an incremental change of body velocity, divided by that incremental velocity":

$$m_a = C_a m_d \quad (11)$$

where $C_a$ is the added mass potential coefficient (in the case of a circular cylinder it can be approximated to unity).

The equation of motion (7) can thus be finally rewritten as:

$$(m + m_a)\ddot{y} + c_{tot}\dot{y} + ky = \frac{2}{\pi D} C_L \sin(2\pi f_V t + \varphi) m_d U^2 \quad (12)$$

The total system damping ratio $\zeta_{tot}$ can be defined as:

$$\zeta_{tot} = \frac{c_{tot}}{2\sqrt{k(m+m_a)}} \quad (13)$$

In the non-linear model $\zeta_{tot}$ is a function of the maximum oscillation amplitude of the cylinder $y_{max}$. In order to determine this function, as suggested in [4] by Bernitsas under the hypothesis of pure harmonic oscillations in lock-up conditions ($f_{cyl} = f_V$), it is possible to integrate both sides of (12) over one single oscillation period $T_{cyl}$, after multiplication by the instantaneous velocity, leading to:

$$\frac{1}{2}\rho\pi C_L U^2 f_{cyl} y_{max} DL\sin(\varphi) = 8\pi^3(m+m_a)\zeta_{tot}(y_{max}f_{cyl})^2 f_0 \quad (14)$$

By recalling the expressions representing the mass ratio $m^*$(5), the lift coefficient $C_L$ (9) and the added mass $m_a$ (11), the system damping ratio $\zeta_{tot}$ can be expressed as a function of $y_{max}$:

$$\zeta_{tot} = \frac{C_L U^2 \sin(\varphi)}{4\pi^3 D(m^*+C_a) y_{max} f_{cyl} f_0} \quad (15)$$

## 3.2. Power and Efficiency

**3.2.1 Power in the fluid:** The kinetic pressure in the fluid stream at infinite distance from the obstacle is given by Bernoulli's equation:

$$p = \frac{1}{2}\rho U^2 \, . \quad (16)$$

The power in the fluid can be calculated considering the aerodynamic force projected on the body cross-section and the mass flow rate per unit section:

$$P_{fluid} = \frac{1}{2}\rho U^3 DL \quad (17)$$

**3.2.2 Fluid Power extracted by the device:** The work done by the transverse fluid force acting on the device during a vibration cycle is obtained from the scalar vector product of the force and of the displacement *dy*, that is, integrating over one cycle the right hand of Equation (12):

$$W_{fS} = \int_0^{T_{cyl}} F_{fluid}\, \dot{y} dt \quad (18)$$

Referring to the synchronization regime, the oscillation period $T_{cyl}=1/f_{cyl}$; after integration, the fluid power extracted by the device can consequently be calculated as:

$$P_{fS} = \frac{1}{2}\rho\pi C_L U^2 f_{cyl} y_{max} DL\sin(\varphi). \quad (19)$$

**3.2.3 Energy conversion efficiency:** The energy conversion efficiency can be calculated as the ratio between the power extracted by the device and the power in the fluid:

$$\eta_{fS} = \frac{P_{fS}}{P_{fluid}} = \frac{\frac{1}{2}\rho\pi C_L U^2 f_{cyl} y_{max} DL\sin(\varphi)}{\frac{1}{2}\rho U^3 DL} \quad (20)$$

# 4. Implementation of the model

In the previous section, the dynamic model and the relationships describing energy extraction from the VIVACE Converter have been developed. The relations describing the equation of motion of the body (12) and the efficiency of the device (20) were implemented into a MATLAB code; consequently a time-domain Simulink model was assembled and validated against the available experimental data; a set of design parameters was then investigated analyzing the effects on device performance.

## 4.1 Input Data

In this first part of the simulation, the input data used in experimental studies in [3] and summarized in Table 1 were chosen. The bluff body was designed as an aluminum cylinder with a thickness of 45 mm, with the idea of generating an internal cavity which could be filled with water from the stream; as a result, $\rho_{cyl}$ is an intermediate value between water and aluminum density. This solution was chosen having in mind - as a future development - to possibly adjust $\rho_{cyl}$ - and consequently the system dynamic response - by filling or emptying the cavity through an appropriate use of a pump and a containment membrane.

*Table1. Input values derived from experimental data of Bernitsas et al.[3].*

| | | | |
|---|---|---|---|
| Cylinder diameter | $D$ | 0.125 | (m) |
| Cylinder length | $L$ | 0.914 | (m) |
| Reynolds number | $Re$ | $0.9\text{x}10^5$ | |
| Stream velocity | $U$ | 0.84 | $(\text{ms}^{-1})$ |
| Cylinder density | $\rho_{cyl}$ | 1430(Al+$H_2O$) | $(kgm^{-3})$ |
| Spring mass | $m_{spr}$ | 1.65 | (kg) |
| Lift coefficient | $C_L$ | 0.50 | |
| Spring stiffness | $k$ | 1000 | $(Nm^{-1})$ |
| Mass ratio | $m^*$ | 1.45 | |

## 4.2 Simulink Model: validation

The Simulink model consists of two sections. The first one, shown in Fig. 3, represents the system dynamics as regulated by (12).

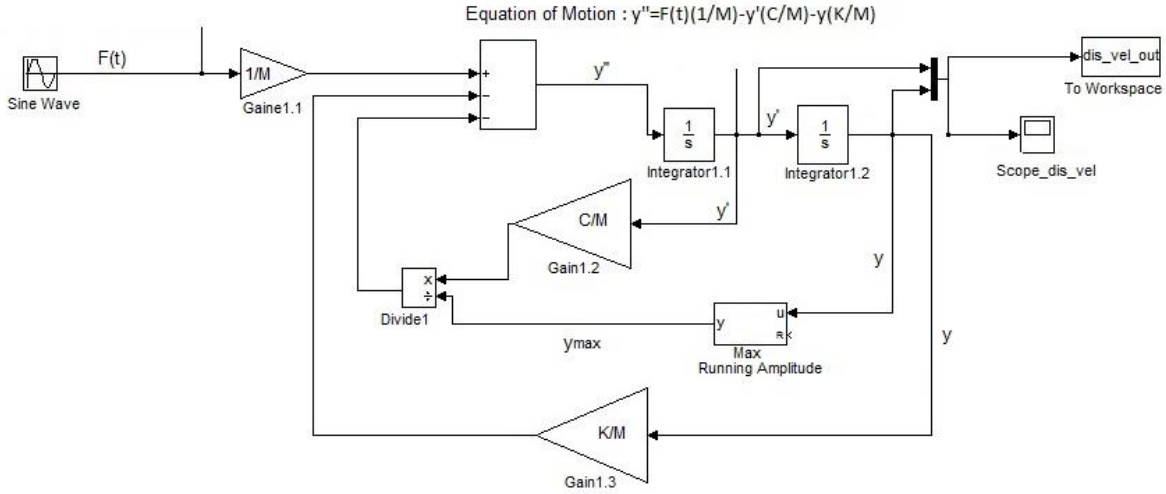


*Fig.3.Schematic of the dynamic Simulink model.*

On the left of Fig. 3 , the external forcing input due to the action of the fluid is entered, while on the right side two feedback loops are represented. The first loop, which refers to the body displacement $y$, is multiplied by the spring stiffness. The second one, which refers to the body velocity $\dot{y}$, is multiplied by the damping. Equation (15) shows that the damping is non-linear as it depends on the maximum oscillation of the cylinder, $y_{max}$, which varies for a certain transitional period before settling at a constant oscillation value. The simulation calculates the term $y_{max}$ and updates its value inside the damping ratio $\zeta_{tot}$ proceeding step by step in time. The results in Fig. 4 show how the oscillation amplitude, after a transient of about 400 s, settles to a constant value.

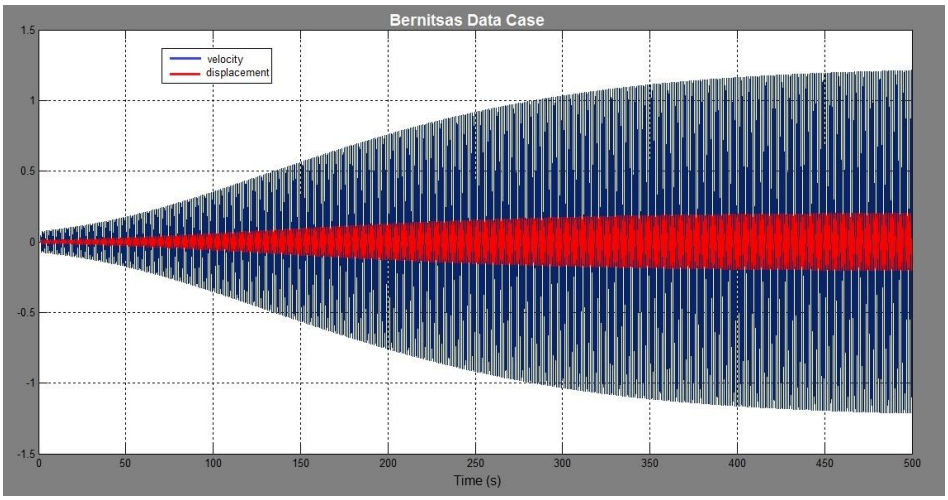


*Fig.4. Simulation results: cylinder velocity and displacement (input data from Table 1).*

A second section of the Simulink code (here not shown as a figure) performs the energy analysis of the model, calculating the power extracted from the fluid $P_{fS}$ (19), and the efficiency $\eta_{fS}$ (20).
The results in terms of $\eta_{fS}$ are shown in Fig. 5, which is in good accordance with the steady-state experimental data [4] (which recorded a value of 38% for a similar experiment).

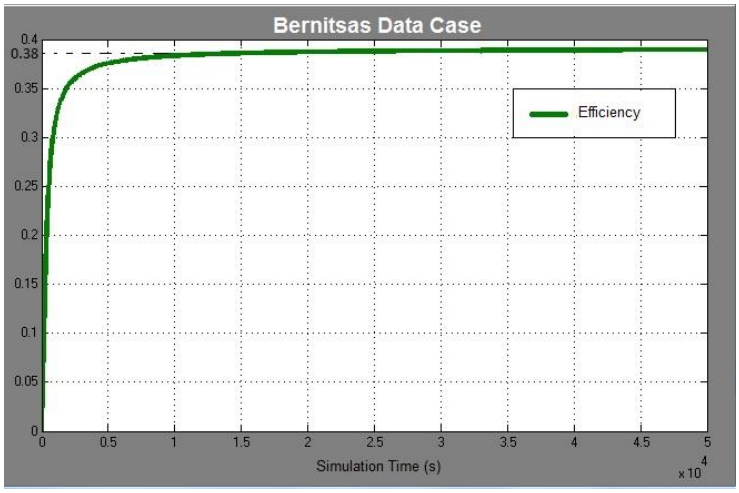


*Fig.5.Simulation results: Energy conversion efficiency $\eta_{fS}$.*

## 4.3 Model Sensitivity Analysis

It is relevant to investigate which cylinder size is advantageous in terms of $\eta_{fS}$ (21), for different values of flow velocity.
The velocity range of the incoming stream can be set between 0.4 and 1.2 m/s, representing realistic values of marine and river currents [11]. Considering this range of fluid velocities, the formula of the Reynolds number produces a corresponding range of diameters.
In terms of cylinder length $L$, from the literature [4] a range of $7 < L/D < 30$ was considered.
In order to maintain the Reynolds number similarity, if the input velocity $U$ increases, the diameter of the cylinder must decrease and consequently also its length. In this way, a sufficient rigidity of the cylinder is ensured, avoiding possible breakage or bending of the oscillating structure.
Lee and Bernitsas [12] have shown that the non-dimensional amplitude $y_{max}/D$ can reach a value of about 1.6-1.8 with suitable tuning of the device. The experiments reported by Bernitsas et al. [3-4] report a spring-mass ratio $6 < k/m < 15$. The spring stiffness values were calculated accordingly, considering the mass of the cylinder.
In Table 2 the suitable ranges of $D$ and $L$ for each velocity are summarized.

*Table 2.Cylinder geometry as a function of input velocity U for Re in the range $10^4$-$10^5$.*

| Input Velocity *U* (m/s) | Diameter *D* (m) | Length *L* (m) |
|---|---|---|
| 0.4 | 0.028-0.28 | 0.8-1.9 |
| 0.5 | 0.022-0.22 | 0.6-1.5 |
| 0.6 | 0.019-0.19 | 0.5-1.3 |
| 0.7 | 0.016-0.163 | 0.45-1.1 |
| 0.8 | 0.014-0.143 | 0.4-1 |
| 0.9 | 0.012-0.127 | 0.35-0.9 |
| 1.0 | 0.011-0.114 | 0.3-0.7 |
| 1.1 | 0.010-0.104 | 0.3-0.7 |
| 1.2 | 0.009-0.095 | 0.3-0.65 |

A series of numerical simulations was performed for each flow velocity *U*, with different values of *D* and *L* within the ranges in Table 2. For each velocity, the results can be summarized as shown in Fig.6, showing $\eta_{fS}$ for a flow velocity of 0.4 m/s; the maximum efficiency is approximately 0.13, and is obtained with a cylinder diameter of 0.28 m and a length of 1.44 m.

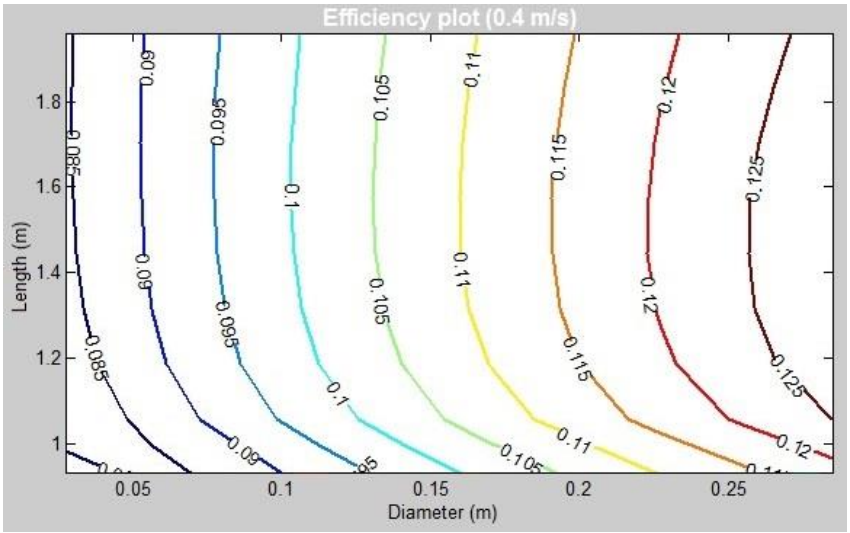


*Fig. 6. Efficiency plot for U = 0.4 m/s.*

The simulation results for the whole set of velocities are summarized in Table 3: for each velocity the maximum achievable efficiency is associated with the cylinder dimensions. In the right column the design spring stiffness is also reported.
From the results summarized in Table 3, it can be seen that the efficiency grows rapidly for increasing values of U, until 0.9 m/s (37%); its increase is slower (up to a value of 48%) for velocity values exceeding 0.9 m/s. It can be concluded that the system can be well adapted to streams having U around 0.9-1.2 m/s, with the typical cylinder geometry ($D\approx$ 0.1 m and $L\approx$ 0.7 m) which is reported by Bernitsas et al. in their experiments [3].

# 5. Application to Mediterranean Sea conditions

The analysis presented in the previous section allows the designer to develop a correct system configuration for a given location and velocity of the stream. In the following section two potentially promising locations in the Mediterranean sea have been considered: the Strait of Messina and the Venice Lagoon.

*Table 3. Maximum efficiency conditions and corresponding system configurations.*

| Stream Velocity $U$ (m/s) | Max efficiency $\eta_{fS}$ | Length $L$ (m) | Diameter $D$ (m) | Stiffness $k$ (N/m) |
|---|---|---|---|---|
| 0.4 | 13% | 1.44 | 0.28 | 1800 |
| 0.5 | 17% | 1.11 | 0.22 | 1200 |
| 0.6 | 21% | 1.07 | 0.19 | 1000 |
| 0.7 | 25% | 0.9 | 0.16 | 800 |
| 0.8 | 32% | 0.8 | 0.14 | 600 |
| 0.9 | 37% | 0.7 | 0.12 | 500 |
| 1.0 | 41% | 0.64 | 0.11 | 400 |
| 1.1 | 45% | 0.58 | 0.1 | 300 |
| 1.2 | 48% | 0.57 | 0.09 | 200 |

## 5.1 The Strait of Messina

The Strait of Messina seems to be the only site in Italy where the stream has an intensity allowing meaningful production of energy from marine currents [13]. As an example, in July 2013 the mean and maximum value of the current are equal to 0.70 and 2.5 m/s respectively at a depth ranging from 10 m to 20 m [13]. The seasonal variation can be evaluated considering the data collected by Istituto Idrografico della Marina [11] (Tab. 4).

*Table 4. Strait of Messina monthly average velocity at a depth of 9 m[11].*

| Month | Average Vel. $\bar{U}$(m/s) |
|---|---|
| January | 0.6 |
| February | 0.5 |
| March | 0.4 |
| April | 0.5 |
| May | 0.6 |
| June | 0.6 |
| July | 0.7 |
| August | 0.4 |
| September | 0.4 |
| October | 0.5 |
| November | 0.5 |
| December | 0.6 |

Considering the above-described experimental data, simulations were performed assuming that the device was installed at a depth of 9 m, with an average stream velocity $\bar{U}$ = 0.525 m/s and a standard deviation σ = 0.09 m/s.

Applying the proposed model, the recommendable dimensions of the cylinder for the mean value of velocity have been determined (Fig. 7). The design configuration was identified as: $D$= 0.21 m, $L$= 1.10 m and $k$ = 1150 N/m.

Under these conditions, the maximum achievable efficiency $\eta_{fS}$ was about 18%. Since the current velocity is variable in reality, simulations were carried out for velocities within the range $\bar{U}\pm\sigma$. In this range, simulations shows that $\eta_{fS}$ varies from 15% to 19%.

Referring to Equation (19), the power produced by a single cylinder is approximately equal to $P_{fS}$= 4.28 W. In order to estimate the power potentially generated by an industrial plant, an energy-harvesting farm using a sea surface of 100 m by 100 m was considered. The maximum number of cylinders that can be mounted on this reference surface was investigated, in order to estimate the power that can be delivered. The farm assembly was designed considering the arrangement constraints reported in [3-4] for an array of converters. Following these guidelines, assemblies with a height $y$ = 5 m and a length $x$ = 5 m, with a width equal to the length of the cylinder ($z$ = 1.10 m) were considered; each assembly composed of a hopscotch array of three rows of four cylinders and two rows of three, as shown in Fig.8, for a total of 18 cylinders. In the reference seabed area it is

thus possible to place 20 rows along *x*, each consisting of 50 modules along *z*, for a total of 1000 units. The complete farm would produce a power of 77 kW.

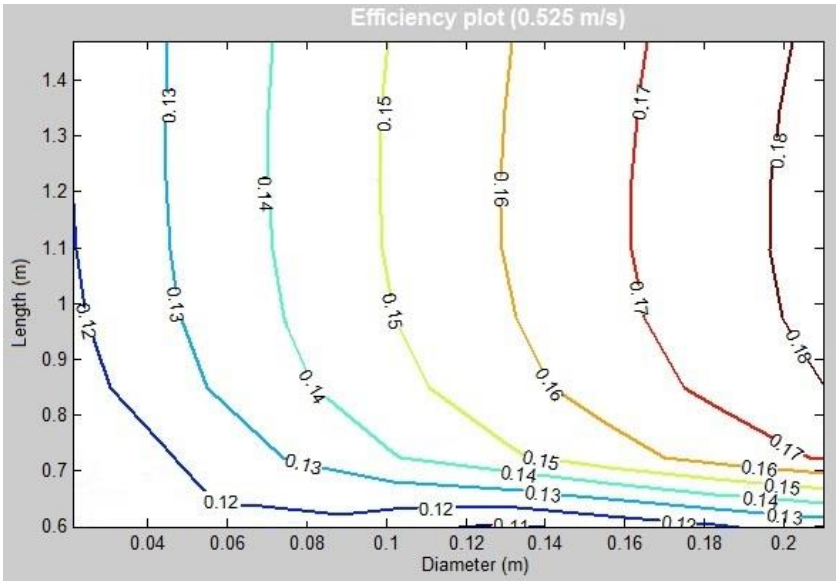


*Fig.7. Efficiency plot for U = 0.525 m/s (Strait of Messina).*

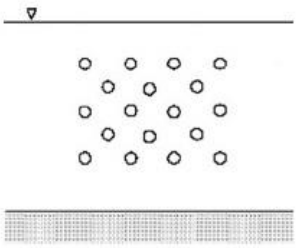

*Fig. 8.Device arrangement for a single assembly.*

## 5.2 The Venice Lagoon

The Venice Lagoon location was been investigated: here the stream velocities are lower, however, considerable volumetric flows are periodically present, and large infrastructures are being completed to regulate them and protect the historical town [14]. The monthly average velocities were again taken from Istituto Idrografico della Marina [11]. The annual average velocity was found to be $\overline{U}$ = 0.375 m/s, with a standard deviation σ = 0.075 m/s. The resulting design geometric dimensions are *D*= 0.3 m, *L*= 1.54 m and *k*= 1900 N/m, with an average power of 2.12 W for a single device.

With this configuration the maximum efficiency $\eta_{fS}$ was found to be about 12% for the mean input velocity. Following the same guidelines as for the Strait of Messina, the configuration for an energy-harvesting farm was identified: since the sea and current characteristic are different, the Venice Lagoon assemblies (always considering a height of 5 m) consist in two rows of three cylinders separated by two rows of two, for a total of 10 cylinders; the farm was again arranged in 20 rows of 50 assemblies, allowing this complete setup to produce an average power of 22 kW. The natural stream appears thus to be too slow to allow a good potential for energy harvesting. The situation should be revised if the devices were integrated within the maritime infrastructures designed for flood protection, determining this a local boosting of the natural stream velocity.

# 6 Conclusions

A non-linear model for the Vortex-Induced Vibration Energy converters was built and implemented into a Matlab/Simulink code. The results were validated against the available experimental model

test data; the sensitivity to the operating conditions (stream velocity) and to the design parameters (Diameter and Length) was investigated.
Two applications for energy-harvesting referring to sea streams existing in the Mediterranean sea were investigated: the Strait of Messina and the Venice Lagoon. These streams are characterized by low velocities ($0.3 < U < 0.6$ m/s) and consequently the efficiency of the device is relatively low (12 to 18%): however this would happen also for traditional devices (turbines), and the VIV concept allows in principle easy replication to cover substantial surfaces (here, a square of 100m*100m was considered) with reasonable costs. The results in terms of power generation potential look quite interesting for the location of Strait of Messina, with an average power yield of 77 kW. The Venice Lagoon location has a substantially lower power yield, if no stream intensification device is applied. Among the future developments, it might be interesting to investigate in detail the flow disturbances due to the cylinders, and their interaction in an hypothetical plant as a function of their spacing.

# Nomenclature

$C_L$ *lift* coefficient
$c$ viscous damping, (N s)/m
$D$ diameter, m
$F$ force, N
$f$ frequency, Hz
$k$ spring stiffness, N/m
$L$ length, m
$m$ mass, kg
$P$ power, W
$p$ pressure, Pa
$Re$ Reynolds number
$St$ Strouhal number
$T$ period, s
$t$ time, s
$U$ stream velocity, m/s
$W$ work, J

**Greek symbols**

$\zeta$ non-dimensional viscous damping
$\eta_{fs}$ efficiency (fluid-to-structure)
$\rho$ density, kg/m$^3$
$\omega$ pulse, rad/s
$\varphi$ phase shift, rad

**Subscripts and superscripts**

$*$ non-dimensional
$\bar{}$ mathematical average
$0$ natural
$a$ added
$addin$ added inertia
$aer$ aerodynamic
$cyl$ cylinder
$d$ fluid displaced

| | |
|---|---|
| *fluid* | fluid |
| *gen* | generator |
| *harn* | harness |
| *max* | maximum value |
| *St* | Strouhal |
| *sys* | system |
| *tot* | total |
| *tra* | transmission |
| *V* | vortex formation |

## References


[1] Bearman P.W., 1984, Vortex Shedding from Oscillating Bluff Bodies. Annual Review of Fluid Mechanics 1984; 16:195–222.

[2] Bernitsas M.M., Raghavan K., Fluid Motion Energy Converter. U.S. Patent Application; 2005, U.S. Patent and Trademark Office Serial No.11/272, 504.

[3] Bernitsas M.M., Ben-Simon Y., Raghavan K., Garcia E.M.H., The VIVACE Converter: Model Tests at High Damping and Reynolds Number Around $10^5$. 25th International OMAE Conference, June 10-15 2007, San Diego, CA.

[4] Bernitsas M.M., Ben-Simon Y.K., Garcia E.M.H., VIVACE (Vortex Induced Vibration Aquatic Clean Energy): A New Concept in Generation of Clean and Renewable Energy From Fluid Flow. ASME Journal of Offshore Mechanics Arctic Engineering 2008; 130 (4).

[5] Khalak A., Williamson C.H.K., Fluid Forces and Dynamics of a Hydroelastic Structure With Very Low Mass and Damping. Journal of Fluids and Structures 1997; 11:973-982.

[6] Sarpkaya T., A Critical Review of the Intrinsic Nature of Vortex Induced Vibrations. Journal of Fluids and Structures 2004; 19 (4):389-447.

[7] Williamson C.H.K., Govardhan R., Vortex Induced Vibrations. Annual Review of Fluid Mechanics 2004; 36:413-455.

[8] Govardhan R., Williamson C.H.K., Modes of Vortex Formation and Frequency Response of a Freely Vibrating Cylinder. Journal of Fluid Mechanics 2000; 420:85-130.

[9] Zdravkovich M.M., Flow Around Circular Cylinders (Fundamentals). Oxford, UK: Oxford University Press. 1997. Vol. 1.

[10] Norberg C., Fluctuating lift on a circular cylinder: review and new measurements. Journal of Fluids and Structures 2003; 17:57-96.

[11] Istituto Idrografico della Marina, Atlante delle correnti superficiali dei mari Italiani. 1982; Genova.

[12] Lee J.H. Bernitsas M.M., High-Damping, High-Reynolds VIV Tests for Energy Harnessing Using the VIVACE Converter. Ocean Engineering Nov. 2011; 38 (16):1697-1712.

[13] Coiro D.P., Lioniello F., Troise G., Misura del profilo di corrente marina nello Stretto di Messina ai fini della stima della produzione di energia. Agenzia nazionale per le nuove tecnologie, l'energia e lo sviluppo economico sostenibile (ENEA). 2013; Report RdS/2013/087.

[14] The official web site of the MOSE - Per la difesa di Venezia e della Laguna dalle acque alte. Available at:<https://www.mosevenezia.eu/>.